

Radiation effects in nanoclusters embedded in solids

Aleksi A. Leino, Flyura Djurabekova, and Kai Nordlund^a

Department of Physics and Helsinki Institute of Physics, P.O. Box 43, 00014 University of Helsinki, Finland

Received 3 June 2014 / Received in final form 26 August 2014

Published online 20 October 2014 – © EDP Sciences, Società Italiana di Fisica, Springer-Verlag 2014

Abstract. Nanoclusters embedded in hard solid materials such as silica show great promise for increased practical applications, as they combine the exciting nanosize effects with very high structural stability. Ion irradiation can be used to tailor the properties of these clusters, the perhaps most dramatic example being the use of swift heavy ions to reshape spherical metal nanoparticles to have antennas or become rods. In this article we review experimental and simulation studies of ion beam processing of nanoclusters embedded in solids.

1 Introduction

The advent of new experimental and computational tools in the 1980's that made the nanoscale more easily accessible, have lead to a dramatic increase of the scientific interest in this size scale. It has also already lead to numerous practical applications: everyday products like sun tan lotion, cosmetics and car wax sold in normal supermarkets already regularly contain nanoparticles of some sort, and carbon nanotubes are used in sports equipment such as icehockey clubs and bicycle frames. However, the most ambitious ideas of nanoscience, such as single-molecule electronics or atom-by-atom manufacturing [1], remain unrealized in practical applications.

One of the exciting possibilities of nanoscience is the use of nanoclusters as part of electronics and optoelectronics. As the silicon integrated circuit industry continuously drives towards smaller and more efficient circuitry [2], the individual parts are already in the sub-100 nm size scale [3]. Further development requires smaller and smaller individual structures, and nanoclusters embedded inside a semiconductor or insulator matrix offer one natural possibility for achieving this. A good illustration of this possibility is that in 1995 it was shown on the laboratory scale that nanoclusters can act as the charge-storing structure in floating gate memories [4,5]. Further developments lead to nanocrystal memories becoming commercially available in 2010 [6], demonstrating that embedded nanocluster-based technologies indeed can lead to commercially viable products.

In fact the use of nanocrystals embedded inside solids offers some major advantages compared to using them in liquid solutions. Inside a solid, the cluster is protected from the environment, especially if the surrounding material does not allow for any significant diffusion of impurities. This will prevent any environmental degradation and thus lead to long-term stability of the cluster. A good ex-

ample that this kind of stabilization can be very durable is the use of nanoclusters to color glassware. This approach was used already in ancient times and lead to glass objects colored by metal nanocrystals stable for millenia [7]. Moreover, the solid ensures the cluster stays in an intact position in the material, and does not coalesce with other clusters. The matrix can even stabilize clusters in nonequilibrium states. A very important example of this is cementite in steels. Even though cementite is in principle metastable alloy, inside an iron matrix it can be stable in the nano- and micron scale, and in fact have a major effect on the hardness of steels [8–10]. However, there are many additional possibilities for which nanocrystals could be potentially used, and intense research is ongoing to explore such possibilities.

A historically completely different branch of science is the study of radiation effects in materials. This field originated more than a hundred years ago, when the existence of X-rays and radioactivity became known, and has since then become a wide multidisciplinary field of science covering both harmful and beneficial uses of irradiation. The former includes e.g. radiation damage in nuclear reactors [11–14], and the latter e.g. cancer treatment [15], using irradiation in plant breeding [16] and the big business of ion implantation of dopants for getting desired electronic functionality in silicon [2,17].

Recently, the studies of nanoclusters and irradiation have started to overlap. As illustrated with bibliographic data in Figure 1, since 1992 there has been a major increase in combined studies of ion irradiation and nanoclusters. Although the range of topics covered in these works is wide, most of the literature found in this search either searches for ways to synthesize nanoclusters with irradiation, or alternatively to modify already existing nanoclusters with it. The ultimate motivation is similar to that for the more conventional ion irradiation of bulk matter: to search for ways in which ion beams can be used to synthesize new materials or modify materials to get new

^a e-mail: kai.nordlund@helsinki.fi

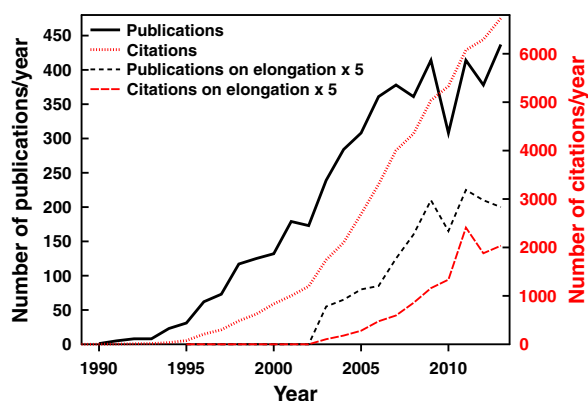


Fig. 1. Results of a Web of Science¹ search carried out on June 1st, 2014, using the advanced search keyword “TS = (“ion irradiation” or “ion implantation” or “ion beam*” or “collision cascade” or “radiation effects” or “swift heavy ion*”) AND TS = (nanocluster* or NC or nanoparticle* or nanocrystal*)”. Also shown is, enhanced by a factor of 5 for visibility, a search for papers on the recent hot topic of elongation of nanoclusters, carried out with the search key “TS = (“ion beam shaping*” OR “swift heavy ion*” OR “ion track*”) AND TS = (nanocluster* or NC or nanoparticle* or nanocrystal*)”. Web of Science covers the titles, keywords and abstracts of all major refereed publication series in the natural sciences since 1949. The search gave in total 4815 hits, but no hit before 1990. The data illustrate that the topic of this review was growing rapidly in scientific interest since 1990, and is still growing.

properties that cannot be achieved with more conventional near-equilibrium approaches. Since irradiation effects can clearly be different from homogeneous bulk even at flat interfaces [18–23], and embedded nanoclusters have a high interface-to-volume ratio, it is natural to expect that radiation effects in embedded nanoclusters can differ strongly from the bulk ones, making the topic very interesting also from a basic science point of view.

As the topic of irradiation effects in nanostructures has been examined for about 20 years now, it is natural it has also been already reviewed from several points of view. For instance, Krashennikov and Nordlund recently reviewed the overall topic of irradiation of any kind of nanomaterial [24], Dhara the ion beam synthesis of nanoclusters in solids [25] and Nordlund and Djurabekova multiscale modelling of irradiation in nanostructures [26]. The aim of the current article is to review specifically the scientific understanding of radiation effects and ion beam modification of nanoclusters embedded in solids, a topic that has been rapidly evolving in recent years. In particular, there has been especially rapidly increased interest on the newly discovered topic of ion beam shaping of nanocrystals, which we pay particular attention to in this review.

The paper is organized as follows: in this introductory section, we still give a brief summary of the topic of nanocluster synthesis with ion beams. In Section 2 we review the ways to control the spatial and size distribution

of nanoclusters, in Section 3 we present the knowledge on radiation damage in nanoclusters, and in Section 4 the ion beam shaping topic. Finally, in Section 5 we give some summarizing notes and outlook.

1.1 Synthesis of embedded nanoclusters by irradiation

Although this is not the main topic of this article, we briefly review the synthesis of nanoclusters in solids by irradiation.

Ion implantation has an important role for the fabrication of nanoclusters embedded in solids: a standard way to achieve this is to implant atoms of a certain type into a matrix with which they are immiscible. After heating to temperatures high enough that the implanted atoms become mobile, they will segregate from the matrix and form nanoclusters if the implantation depth is suitable compared to the migration distance, see Figure 2 [27,28]. This topic has been studied extensively both by experiments and simulations (see e.g. [27–33]). Since this way of synthesizing embedded nanoclusters has been recently reviewed elsewhere, [34] we will not review the fabrication of nanoclusters with implantation in detail, but instead focus on reviewing the ion modification of embedded nanoclusters and nanoparticles *after* they have been synthesized.

It is, however, important to realize that embedded clusters can also be made with a variety of other techniques, such as thermal decomposition of thin grown layers [35,36] or co-sputtering [37]. Conceptually the simplest approach is to deposit chemically synthesized nanoparticles onto a surface, then overgrow the deposited area with additional matrix material [38]. This has the advantage that the depth distribution of the particles is very well defined. Moreover, the approach also allows for very good size control in case the initial chemically synthesized particles have a narrow size distribution. For instance, in reference [38] Au and Ag particles with a size dispersion of 10% around the nominal value were embedded in silica at a well-defined depth of 300 nm. On the other hand, in this approach the nanoclusters can get oxidized or otherwise contaminated from the surrounding before they are embedded in the solid. In some special cases, also ion irradiation can achieve a very well-defined depth and size control, as discussed in Section 2.2.

Regardless of synthesis method, the end result is typically roughly spherical nanoclusters with sizes ranging from just a few atoms [39] to ~100 nanometers [38]. These nanoclusters can be further modified by ion irradiation, as discussed in the remainder of the review.

2 Distribution control by ion irradiation

2.1 Inverse Ostwald ripening

A key aspect of nanocrystal growth occurring under any condition is the Ostwald ripening process [40]. In it, small particles are more likely than big ones to emit atoms or molecules, due to their higher surface curvature, which leads to growth of the large particles at the expense of the

¹ ISI Web of Science (formerly known as Science Citation Index), isiwebofknowledge.com. Web of Science is a registered trademark of Thomson Reuters Inc.

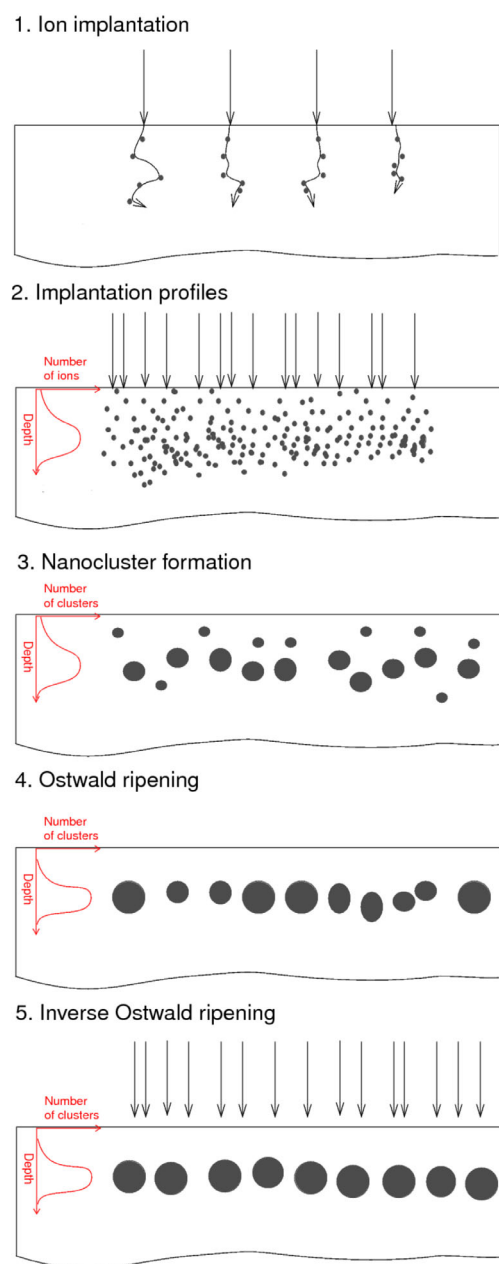


Fig. 2. Schematic of how nanoclusters can be grown by ion implantation, and further modified by Ostwald ripening and inverse Ostwald ripening. Parts 1-2: conventional ion implantation is used to implant impurities into a solid up to high fluences. Part 3: if the implanted material is immiscible in the matrix, it will start precipitating out from it to form nanoclusters. This process is usually facilitated or sped up by annealing. Part 4: if the temperature is high enough, the precipitated clusters have some probability to also emit atoms. This probability is higher for smaller clusters due to higher surface curvature, leading to the growth of the larger clusters and vanishing of the smaller ones, which is the Ostwald ripening effect [40] Part 5: if high energy ion irradiation is carried out during or after the growth, the larger clusters are more likely to emit atoms than the smaller ones due to a large cross section for sputtering, driving the size distribution towards monodispersity. Reprinted with permission from reference [24]. Copyright 2010, AIP Publishing LLC.

small ones [40]. This process happens in a wide variety of conditions, many of them completely unrelated to irradiation; it explains for instance why ice cream tends to get larger grains if poorly refrigerated [41,42]. It can also occur during ion irradiation of nanoclusters (see illustration in Fig. 2), and in that case can be used to increase the size of nanocrystals. It does, however, not lead to a monodisperse size distribution.

The Ostwald ripening of nanoclusters has been examined systematically with a combination of experiments, analytical theory and kinetic Monte Carlo simulations [31,43,44] (although in these simulations, the jump selection rule was the simplified Metropolis rule which does not necessarily account for the migration jump barrier [26,45–48]). It has been shown that by carrying out irradiation on existing nanoclusters, one can achieve an inverse Ostwald ripening process where high energy ion irradiation of existing nanocrystals can, at least under suitable energy deposition conditions, be used to reduce the size of the largest nanoclusters. This is because a competition between the irradiation-induced detachment and the migration leads to a steady state condition where the system wants to achieve a maximal interface area for a given amount of matter. This condition is reached at a monodisperse size distribution [44,49]. In practice, however, the large clusters tend to become surrounded by smaller satellite clusters, at least for the Au in SiO₂ system [43]. It has also been shown that the mechanisms can be utilized to fabricate a thin layer of nanoclusters just above a flat interface in a semiconductor device, see Figure 3 [44].

Inverse Ostwald ripening was also observed in reference [50], where it was shown that an initial Au cluster size distribution with diameters between 2 and 8 nm can be reduced into one with clusters only between 2 and 3 nm, eventually leading to complete dissolution of the clusters. Another study of this process showed that as an intermediate stage, one can obtain a bimodal size distribution of small and large nanoclusters [51].

In summary, inverse Ostwald ripening is a process by which the size distribution of nanoclusters can be controlled, and is reasonably well understood by combinations of simulations and experiments.

2.2 Interfacial control

Under certain conditions, the spatial distribution of nanoparticles can be highly controlled even using the ion implantation approach, even though the initial implantation distribution is broad. In 1997 it was reported [52] that if a silicon wafer irradiated with chemically active Sn ions silica films are left to age at elevated temperatures for long time, the photoluminescence of such samples is significantly more stable than that of similar, but non-aged wafers. The high temperature short term annealing was performed for both samples, aged and non-aged, similarly. The structural analysis showed that the nanoparticles after aging for long time (up to 1 yr) partly evaporated, but mostly created a densely populated two-dimensional array at the interface of SiO₂/Si.

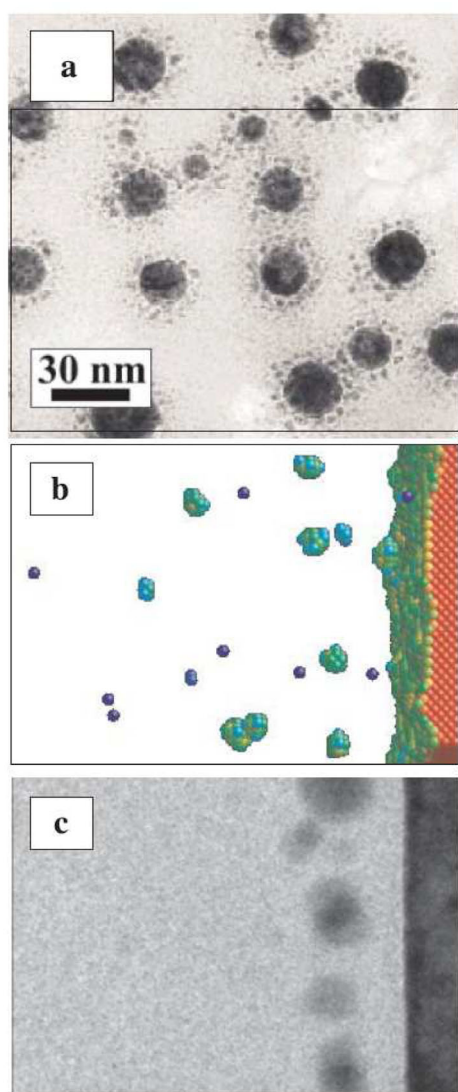


Fig. 3. Formation of nanocrystals at slightly curved or flat interfaces under ion irradiation. (a) TEM image of small Au nanocrystals in SiO₂ formed around large Au inclusions by 4 MeV Au ion irradiation. (b) Kinetic Monte Carlo simulation of ion irradiation of a flat interface. Small nanoclusters appear in front of the interface. (c) Cross-sectional TEM image of a layer of Sn nanoclusters in SiO₂ separated a few nm from the Si/SiO₂ interface. Reprinted from reference [44] with kind permission from Springer Science and Business Media. Copyright Springer.

This effect was confirmed later by [53,54] for the Pb irradiation of silica films, as shown in Figure 4. Moreover, in [54] the authors analyzed the shape of Pb nanoparticles and found that the shape consistently forms a spherical dome on the silica side and a faceted base of notably smaller size, where the crystalline silicon surrounds it. The bubbles observed in the non-aged, but annealed long at high temperature samples, were not seen in the aged nanoparticles. This proves that the aged particles do not undergo the formation of large liquid particles as those annealed at high temperatures for a long time annealing.

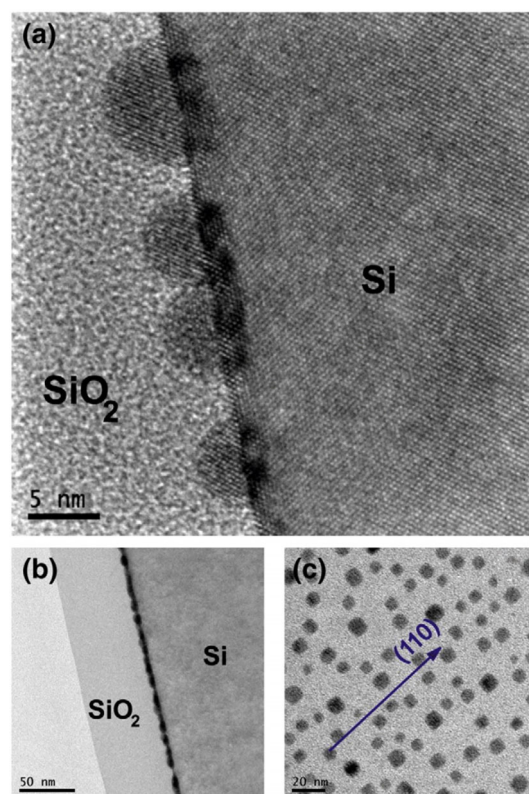


Fig. 4. Pb nanoclusters on a SiO₂/Si interface formed by Pb ion implantation and annealing. (a) Shows an atomic-resolution image demonstrating that the Pb is in crystalline form, and (b) that all Pb indeed is at the interface. (c) Shows an image from the top showing that the clusters are separated and faceted. By selecting a suitable annealing conditions and utilizing the interface, the authors were able to form a monodisperse size distribution at the interface based on a conventional ion implant. Reprinted from reference [54] with permission from Elsevier.

The formation of two dimensional arrays was proven to have a little size dispersion and short range order in a planar structure [53].

3 Radiation response of embedded nanocrystals

3.1 Si nanocrystals in silica

The initial studies of irradiation of embedded nanocrystals was carried out in 1999, when 30 and 130 keV He as well as 400 keV electron irradiation of Si nanocrystals in silica (“NC-Si/SiO₂”) was examined [55,56]. This electron irradiation was reported not to lead to significant damage in the nanocrystals. Transmission electron microscopy (TEM) analysis of the ion irradiated samples showed that the nanocrystals were amorphized by a He dose of the order of 10¹⁶ ions/cm², translating to about 1 displacements-per-atom (dpa). The visible PL was reported to decrease and vanish after a He dose as low as one displacement-per-nanocrystal. This effect was attributed

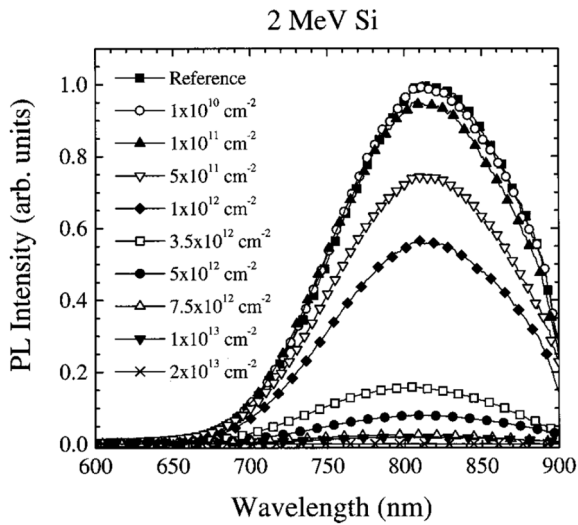


Fig. 5. PL spectra of a SiO_x film with 39 atomic % Si irradiated by a 2 MeV Si ion beam at different fluences. Reprinted from reference [58] with permission from the authors. Copyright (2002) by The American Physical Society.

to production of defect-induced non-radiative recombination centers, possibly situated at the Si nanocrystal/ SiO_2 interface [55]. Annealing at 600 °C was reported to restore the PL to pre-irradiation levels [55]. On the other hand, a higher-temperature (1000 °C) anneal was reported to be necessary to recrystallize the samples [56]. Remarkably, after this annealing the PL intensity was reported to be higher than before the irradiations.

Around the same time, Si nanocrystals embedded in silica were irradiated with 400 keV or 3 MeV Si ions [57]. The irradiation reduced the nanocrystal-related luminescence at a wavelength of 806 nm down to 4% of the initial value for a dose of 5×10^{12} ion/cm². The reduction saturated at a dose of 5×10^{13} ion/cm² (0.18 dpa), which was attributed to amorphization of the cluster at about this dose. On the other hand, the irradiation was also reported to lead to defect emission at a wavelength of 640 nm.

The same NC-Si/ SiO_2 system was also subjected to irradiation by 2 MeV He, Si, Ge and Au ions [58,59]. Similarly to the other works, a strong decrease of the NC-related PL intensity was reported (see Fig. 5), but this drop was also found to be accompanied by a radiative lifetime quenching. This observation was attributed to damage left by the beams (see Fig. 6) [58]. Studies of the nanocrystals after the irradiations indicated that the recovery of the PL properties of completely amorphized Si nanoclusters could be characterized by a single activation energy of 3.4 eV (Ref. [59]). This energy was associated with the transition between amorphous and crystalline phases of each Si grain.

Other studies of the same system include 150 keV P ion irradiation followed by annealing at 100 °C [60], which was reported to enhance the PL intensity without a significant shift in the emission peak position. A special variation of the processing conditions was post-implanting of the Si nanocrystals with 100 keV Si ions (the same en-

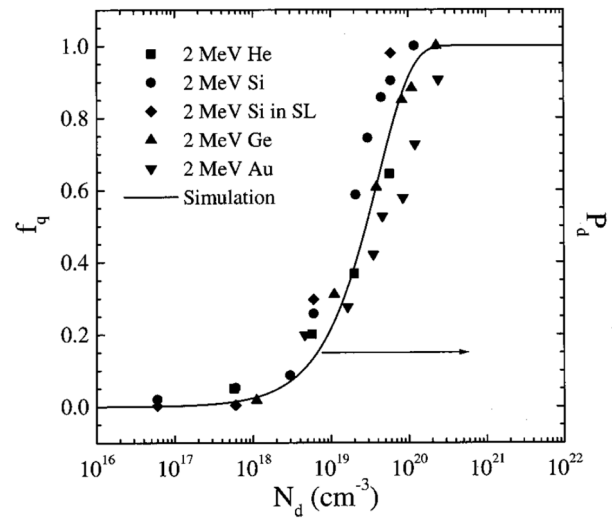


Fig. 6. Fraction of quenched Si nanocrystals f_q vs. defect concentration N_d left over by the ion beam for a Si/ SiO_2 superlattice. The continuous line is a calculated probability P_d of a nanocluster having at least one defect in its volume. This was reported to provide evidence that the quenching can be explained by the nanocrystals having a single radiation-induced defect. Reprinted from reference [58] with permission from the authors. Copyright (2002) by The American Physical Society.

ergy that was used in the synthesis of the crystals), thus leading to energy and ion deposition at exactly the same depth as the nanocrystal layer [61]. This irradiation was reported to lead to full or partial quenching of the PL signal, attributed to defect generation in the crystals.

Also 90 MeV Kr and 130 MeV Xe swift heavy ions (SHI's) have been used to irradiate the NC-Si/ SiO_2 system, after which measurements were made of the current-voltage and capacitance-voltage characteristics at different frequencies [37]. This was reported to indicate the formation of arrays of nanocrystals along the ion tracks.

As noted in the introduction, ion beams are routinely used to introduce dopants into bulk silicon to modify its electric properties. Very recently, by using co-implantation of Si and P or As in silica followed by a single annealing steps, formation of doped Si nanocrystals was achieved [62]. Atom probe tomography demonstrated that P and As dopants were indeed introduced into the nanocrystals. Moreover, it was shown that the dopants do indeed modify both the optical and electrical properties of the Si nanocrystals [62].

3.2 Ge nanocrystals in silica

Using Ge nanocrystals instead of Si provides the advantage that the crystals can be characterized by X-ray methods such as EXAFS and XANES [63,64]. Based on such studies, it was reported that as-prepared nanocrystals already show a high degree of disorder as measured by the EXAFS Debye-Waller factor [63,64]. 5 MeV Si irradiation of the nanocrystal layer was found to lead to the

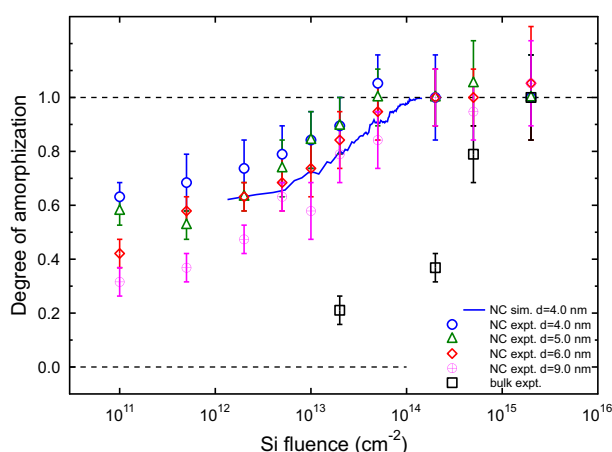


Fig. 7. Amorphization of Ge nanocrystals and bulk Ge by 5 MeV Si ions measured by the EXAFS Debye-Waller factor. Also shown are results from molecular dynamics simulations [65] for the same system. Figure courtesy of M. Backman. Copyright (2009) by The American Physical Society.

amorphization of the nanocrystals at about two orders of magnitude lower doses than for bulk Ge (see Fig. 7).

Molecular dynamics (MD) simulations have been used to examine the amorphization of nanocrystals in silica [66,67]. Atomic models of Si and Ge nanocrystals of the same sizes as those studied experimentally [68] were first created, and the response of these to irradiation was subsequently simulated by starting self-recoils in and near the nanocrystals. The results showed that already the as-prepared interfaces had a fairly high fraction (about 10%) of coordination defects, and that irradiation does not substantially increase the fraction of defects at the interface [66]. While this result may seem contradictory to the experimental results cited above, it should be noted that not all defects are optically active, and in experimental situations many coordination defects are likely passivated by hydrogen. It was also reported prolonged irradiation leads to the amorphization of the nanocrystals at doses considerably lower than those needed to amorphize bulk Si or Ge [65,67] (see Figs. 7 and 8), in good agreement with experimental observations.

It has also been shown that Ge nanocrystals can be doped with Er to form erbium oxide phases, which promote electroluminescence (EL) [69]. For higher annealing temperatures, also the formation of Er_2O_3 nanocrystals and an $\text{Er}_2\text{Ge}_2\text{O}_7$ phase has been reported. These phases were found to diminish the EL, and an Er content of 0.5% was reported to be optimal for maximizing the luminescence.

To summarize these subsections on Si and Ge, the reviewed literature shows that there is clear evidence that ion irradiation of nanocrystals strongly reduces the PL intensity for Si nanocrystals in silica, but that post-irradiation annealing can be used to recover – and in some cases even enhance – the luminescence above the initial levels. The details seem to be very sensitive to the ways of processing the samples before and after irradiation.

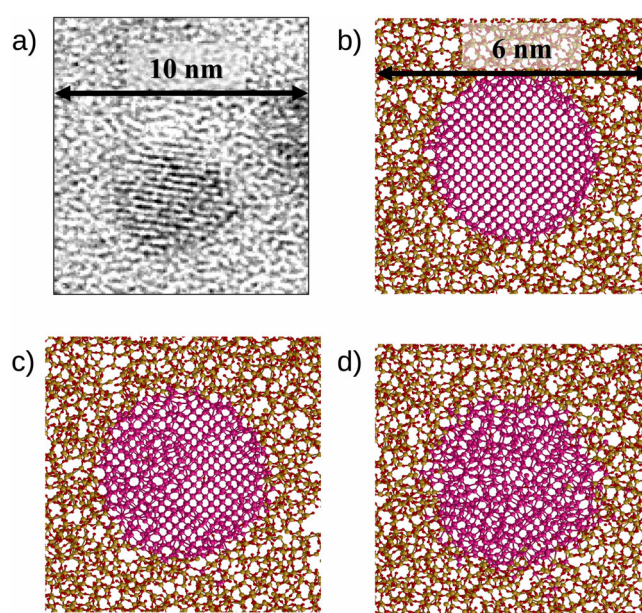


Fig. 8. Amorphization of a Ge nanocrystal embedded in silica. (a) Experimental TEM image of Ge nanocrystal in silica, (b) initial state in simulation, (c) modification after irradiation dose of 1.7 eV/atom, (d) modification after a dose of 4.0 eV/atom. The data for the figures are from references [65,67].

tion. The embedded Si and Ge nanocrystals amorphize at much lower doses than the corresponding bulk material.

3.3 Metal nanocrystals

Radiation effects in Cu and Au nanocrystals embedded in silica have been examined in reference [70]. It is well known that pure elemental metals cannot be rendered amorphous even by extremely large irradiation doses [12,71]. Thus it came as something of a surprise when it was shown that pure Cu nanocrystals with diameters of the order of 3 nm could be amorphized by MeV Sn irradiation [70]. On the other hand, Cu nanocrystals with a diameter of 8 nm were reported not to be amorphized, thus showing explicitly where the limit for nanosized interface-dominated effects with respect to amorphization lies [70]. The disordering of Au nanoclusters in silica was also examined [50,72] and it was shown that Au nanoclusters can be dissolved into Au monomers and very small clusters (dimers, trimers) in the SiO_2 matrix, similar to the small clusters produced around bigger ones in Figure 3. On the other hand, irradiation of 3-dimensional arrays of about 3 nm diameter Co nanoparticles in silica with 90 and 150 keV Ar and characterization of them with RBS and magnetic methods indicated that these nanoparticles had a very high resistance to radiation damage, surviving damage up to 33 dpa [73].

The effects of SHI's on metallic nanoparticles in an Al matrix have also been studied [74]. The results showed that 30 MeV C_{60} cluster ions induced amorphization of the core of about 6 nm diameter Bi nanocrystals, but that

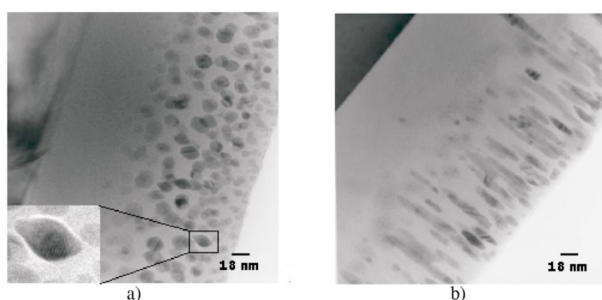


Fig. 9. TEM images of initially spherical Co nanoclusters irradiated by (a) 10^{13} 200 MeV I ions/cm² and (b) 10^{14} ions/cm². Reprinted from reference [76] with permission from the authors. Copyright (2003) by The American Physical Society.

Pb nanocrystals of about the same size were not modified. This was attributed to overpressure being created at the particle-matrix interface.

Comparison of these results indicates that the issue of when elemental metal nanoparticles can be amorphized is complex, and further studies are needed before full understanding of the issue or even a predictive model can be developed.

Co-ion implantation of both Au and Er in silica has recently been shown to have promising optical effects [39]. By implanting Au in such a way that it formed ultra-small metal nanocrystals (in some cases comprising less than 10 atoms) in the same depth region with the implanted Er, the Au clusters were shown to sensitize the photoluminescence of the Er in such a way that intense light emission could be achieved [39,75]. Similar co-implantation of Au and Fe was also shown to lead to 4–6 nm Au-Fe nanoparticles with ferromagnetic properties [75].

4 Ion beam shaping of nanoclusters

SHI's can be used to elongate metal nanoparticles in the direction of the ion beam (see Figs. 9–12). This was first demonstrated in 2003 when 10 nm diameter Co nanoparticles in silica were irradiated with 200 MeV I ions [76]. It was reported that at a fluence of 10^{13} ions/cm², the nanoparticles had prolonged along the incident beam direction into a prolate shape. At a fluence of 10^{14} ions/cm², they had elongated to be on average about 4 times longer than wide (see Fig. 9). This surprising finding has rapidly attracted a flurry of research activity and has posed a great challenge for theoretical interpretation [38,74,76–129].

A wide range of metals can be elongated with a suitable irradiation condition. While Au [38,82,83,85,86,90–93,99,101,103,105,107,108,110–112,115–117,123,128,129] clusters have been most extensively studied, the effect has been repeated using at least Ag [109,118,124,125], Bi [113], Co [76,87–89,94,102,113,114,126,127], Cu [113], Ni [104,113], Pb [113], Pt [95–97,113], Sn [98,113], V [77,80] and Z [77,78,80,113] nanoclusters and a few compound nanoparticles, i.e. Au_xAg_y [38,117] and ZnO [79], in a silica matrix. A similar effect has also

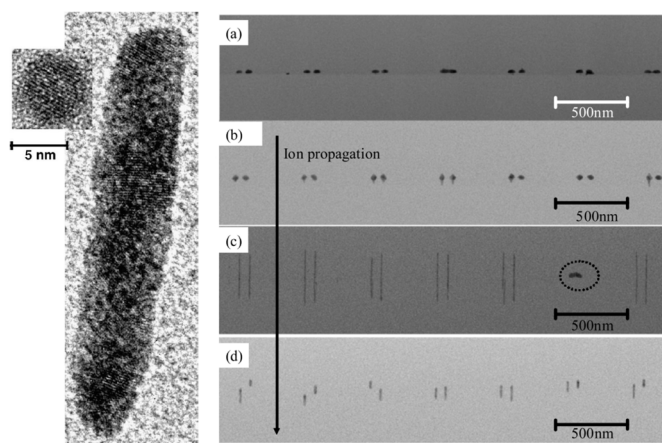


Fig. 10. Left: TEM image of Pt nanoparticles before and after 185 MeV Au irradiation. Reprinted from reference [114] with permission from Elsevier. Right: Irradiation of Au nanodisks ($d = 40$ nm) prepared by electron beam lithography. Shown are initial disks (a) and the end result after irradiation with flux of 3×10^{10} cm⁻² s⁻¹ (b), 6×10^{10} cm⁻² s⁻¹ (c), 16×10^{10} cm⁻² s⁻¹ (d), at a constant fluence of 2×10^{14} cm⁻². From reference [86]. Reprinted with permission.

been seen in FePt particles using alumina as the host matrix [121,122]. In addition to the findings in metals or their oxides, it is known that irradiation of Ge particles with SHI's may result in similar shape transformation [81,119,120] or flattening in the ion beam direction (see Fig. 13).

The elongation effect is interesting from the theoretical point of view, as it is initiated by the electronic excitations of SHI's. Furthermore, once understood, the method could become an alternative to the standard lithography methods [38], as it can be used to produce large arrays of equally aligned nanoparticles which is difficult to achieve otherwise. The elongated particles are stable at room temperature and in some cases even at temperatures exceeding the melting point of the metal nanoclusters [80]. The method has been used to control the location of the surface plasmon resonance peak [107,125], showing promise for applicability in fabricating plasmonic devices. Complete description of the shape transformation from the irradiation conditions to the expected end result is not yet available, but certain characteristics are already well-known.

The elongation effect is initiated in the excitation of the electronic subsystem, as even at the lowest ion energies (e.g. 8 MeV Si in Ref. [109], 10 MeV Si in Ref. [110], 10 MeV Cu in Ref. [90]) that produce the shape transformation, electronic stopping power is clearly dominating over nuclear stopping. Irradiation at lesser energies, where electronic stopping does not dominate anymore, resulted in a ring of small nanoparticles around the main cluster (e.g. 3 MeV Au in Ref. [116]), probably due to the same reason of nuclear recoiling as in inverse Ostwald ripening (cf. Sect. 2.1). Irradiation of 20–80 nm Au nanoparticles with 90 MeV Cl, 100 MeV Cu and 110 MeV Br ions showed that the Cl ions produced no elongation, whereas Cu and Br did [130]. This showed that the lower

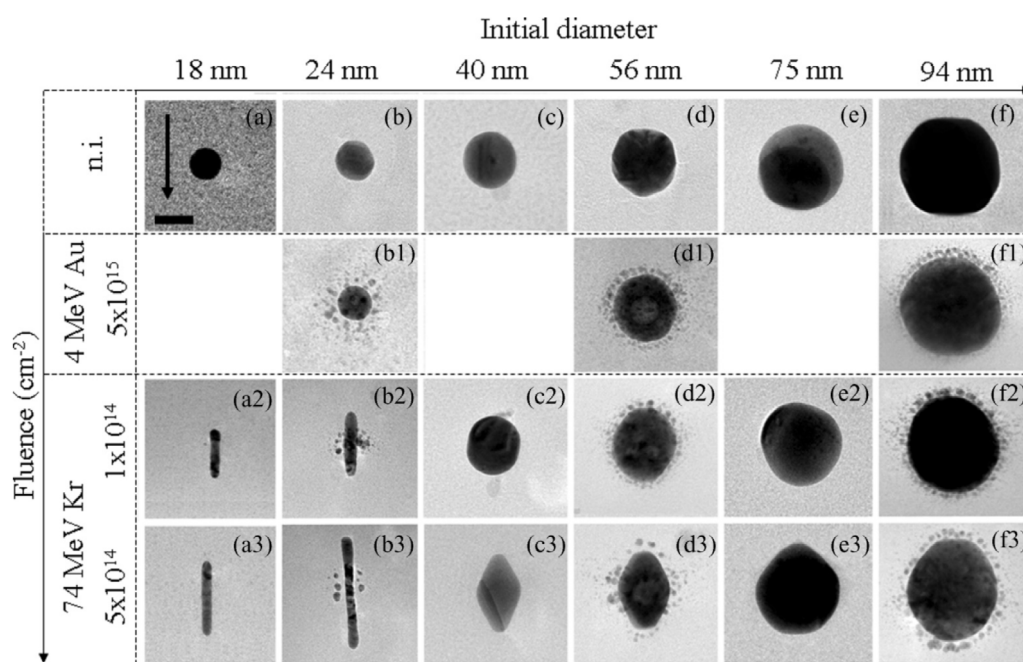


Fig. 11. A diagram showing the morphological changes of Au nanoclusters as a function of particle size and irradiation fluence. Note that some of the clusters have been preirradiated with 4 MeV Au ions to create a halo of small nanoparticles around the main cluster. Reprinted from reference [38] with permission from the authors. Copyright (2012) by The American Physical Society.

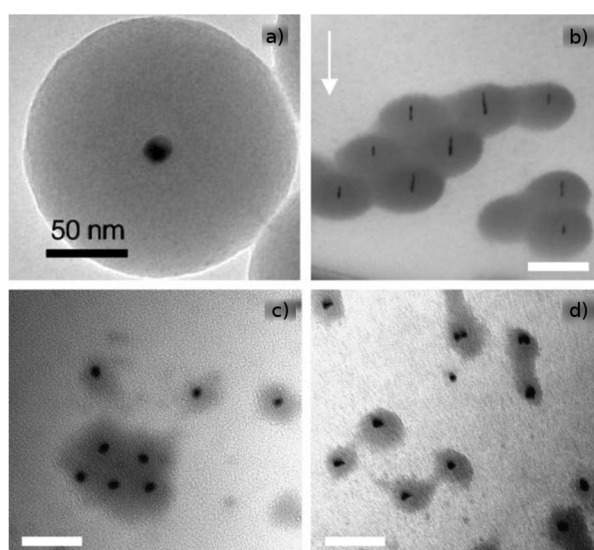


Fig. 12. Irradiation of Au-silica core-shell nanoparticles. (a) Unirradiated nanoparticle ($d_{\text{Au}} = 14$, $t_{\text{SiO}_2} = 72$ nm). (b) After irradiation with 30 MeV Cu ($d_{\text{Au}} = 14$, $t_{\text{SiO}_2} = 65$ nm, 1×10^{15} ions/cm²). (c) $t_{\text{SiO}_2} = 26$ nm, 2×10^{14} ions/cm². (d) $t_{\text{SiO}_2} = 29$ nm, 2×10^{14} ions/cm². White scale bars are 100 nm long. Reprinted from reference [111] with permission from Elsevier.

energy deposition density by Cl was not sufficient to induce elongation.

Along the same lines, using both Ag (12–54 MeV) and Au (10–45 MeV) ions, a threshold electronic stop-

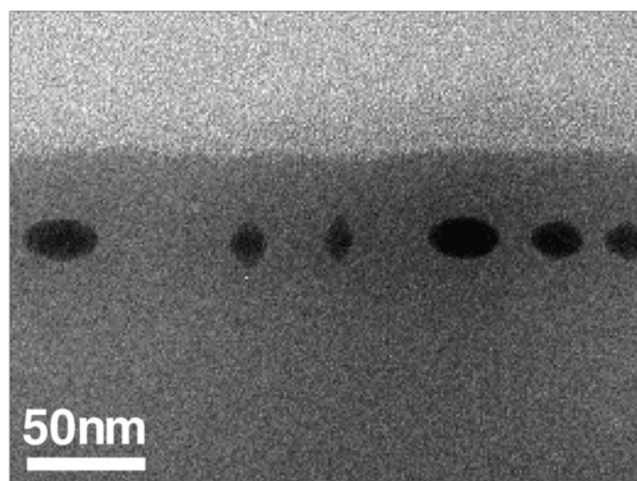


Fig. 13. High resolution cross sectional TEM images of initially spherical Ge nanoclusters after irradiation with 38 MeV I ions at a dose of 1×10^{15} cm⁻². For smaller particles, the major axis is in the direction of the ion beam, whereas in the larger nanoclusters it is perpendicular to the beam. From reference [120], reprinted with permission from Elsevier.

ping power in silica for the elongation effect was extrapolated, below which the Au nanoclusters remained spherical [90]. This threshold was found to be dependent on the particle size ($d = 15$ –80 nm) and was higher for larger particles. A value of 3.5 keV/nm was deduced for nanoclusters with $d = 15$ nm. A similar value of 3.3 keV/nm was found in reference [111] for silica shell-Au core colloidal

particles with identical size. In reference [101], a value of (2.0 ± 0.5) keV/nm was deduced for polydisperse particles with $d < 14$ nm [101].

Several independent works indicate (with an exception given in Ref. [101]) that the rate of the shape change (i.e. the change in aspect ratio with a certain irradiation fluence) increases by increasing the electronic stopping power [90,101,107,117,125]. It remains difficult to make a separation between increment in the stopping power of the metal cluster and the host matrix.

In reference [76] it was reported that at low fluences (3.0×10^{13} ions/cm²) Co particles remained spherical but grew in size. A minimum threshold fluence for Au nanoclusters was observed in reference [91] below which the nanoclusters ($d = 15$ – 45 nm) remained spherical. This threshold was found also to be dependent on the particle size and was higher for larger particles (e.g. 3.0×10^{13} ions/cm² at $d = 15$ nm and 5.0×10^{13} ions/cm² at $d = 30$ nm for 24 MeV Ag). The threshold was decreased by increasing ion energy, so that small particle size ($d = 15$ nm) combined with high ion energy (54 MeV Ag) led to no observable threshold fluence. Similarly, an independent study in reference [101] for particles with diameters less than 14 nm showed no threshold fluence for the shape transformation.

Above the minimum fluence, the aspect ratios of the irradiated particle grow as a function of given total fluence until a saturation fluence was reached, above which no further shape change is seen [91,101,103,113]. This fluence depends on the ion energy and particle size [91,101]. Moreover, it was shown in reference [91] that the saturation fluence depends on the areal density of the clusters. At small fluences the particles seemed to elongate irrespective of the concentration, while at high fluence the samples with lower areal density showed saturation, whereas the ones with highest densities did not. This suggests that at high fluence, the shaping effect can be a collective process involving mass transport between the particles. In contrast, at low fluence, the inspection of TEM micrographs suggested that the nanoclusters elongate under volume conservation and that each particle is shaped individually. It should also be pointed out that no direct evidence exists thus far to suggest that the mass transport observed at high fluence between the elongating particles is directly related to the elongation effect itself, and not a consequence of the regular irradiation assisted Ostwald ripening of the particles.

The individual nature of the elongation process was also seen by other, independent experiments. In reference [131], by using Monte Carlo simulations and optical measurements, it was shown that individual impacts to Zn clusters can cause their shape to change. In reference [86], Au nanodisks with a relatively large separation were fabricated by electron beam lithography to avoid complications due to interactions between the particles. A strong elongation effect was nevertheless observed (see the right side of Fig. 10).

The effect of the flux on the elongation effect was studied in reference [86] using gold nanodisks of 40 and

70 nm in diameter while keeping the fluence constant (2×10^{14} cm⁻², 110 MeV Br). At 3 ions/cm⁻²s the particles had undergone only minor shape change, but by increasing the flux to 6 ions/cm⁻²s the disks had turned into long rods (see Fig. 10). When the flux was further increased to 15 ions/cm⁻²s, the disks appeared to have partially dissolved in to the silica matrix and changed their position. The authors also monitored the temperature of the samples in situ, which showed that the temperature of the sample rises as a function of flux, and that it had risen about 200 K during the irradiation at the highest fluence.

Several works indicate that the smallest particles are not elongated or elongate at considerably lesser rate [88, 98,103,107,113,124]. It has been reported that the smallest particles either grow [88,107] or lose volume [114,124] as a result of SHI irradiation. Moreover, it was shown in reference [103] that there is a correlation between the minor axis of Au nanoclusters and the SHI track diameter in silica. After reaching the saturation fluence, none of the particles had a width larger than the SHI track width in silica, and the width of the majority of the nanoclusters was almost identical to the track width. In reference [113], a systematic study on the saturation width of different nanocluster species was performed. While in several metals (Zn, Bi, Pb, Ag, Sn, Au) the saturation width was comparable to the track diameter in accordance with the earlier reports, in some materials (Cu, Ni, Co, Pt) a shorter saturation width was seen.

The dependence of the metal species of the nanoparticles on the elongation effect has been demonstrated by several authors, but thus far there is no clear understanding of how thermo-mechanical properties of the metal species are linked the elongation effect. Irradiation of Au nanoclusters (30 MeV Si at $1.6 \times 9.3 \times 10^{14}$ ions/cm²) in reference [111] led to prolate shape change but corresponding irradiation of Ag nanoclusters did not. Thus one finds that the efficiency of the shape transformation varies with metal species. It was later, however, demonstrated that Ag nanoclusters can be elongated [109,113,118,124], and it was reported that e.g. 8 MeV Si irradiation of slightly smaller nanoclusters at a higher fluence of about 20×10^{14} ions/cm² led to a shape change [109]. At the moment it remains unclear if Fe nanoparticles can be elongated as irradiation of Fe nanoclusters with 100 MeV Au at 1×10^{13} ions/cm² did not lead to shape change [132]. It was reported in reference [131] when irradiated with almost similar irradiation conditions, the aspect ratio of Zn nanoclusters grew to 1.2–1.7, whereas in Co it grows to 4–5. On the other hand, it was reported in reference [77] that both V and Zn showed comparable elongation, irrespective of the large differences in their melting point.

In reference [123], the structure of elongated Au nanoclusters was examined. Both single crystalline and twinned structures were observed in the bulk fcc configuration.

In more complex systems, the swift heavy 210 MeV Xe ion irradiation of about 2 nm diameter FePt nanoclusters embedded in alumina was reported to cause particles in the film interior to become elongated, with the particle

centers being enriched with Pt [122]. Irradiation of ZnO particles in amorphous SiO₂ with similar ions resulted in deoxidation and elongation of the clusters, so that the elongated particles consisted of Zn [79].

It has also been shown that 80 MeV oxygen ions could modify CdS nanoparticles into elongated structures such as needles and rods [133].

The elongation effect has also been observed Au-silica core-shell colloidal nanoparticles [111]. Irradiation of $d = 15$ nm Au cores with 30 MeV Au led to the deformation of the cores only if the silica shell was made thick (>20 nm, see Fig. 12). Irradiation with 30 MeV Xe led only to an oblate deformation of the silica shell that can be explained by the viscoelastic model, which showed that the two are at least not directly related.

4.1 Proposed mechanisms of elongation

The elongation mechanism of metal clusters was first studied in reference [76]. By a calculation utilizing the thermal spike model as described in reference [134], it was shown that the cluster can melt upon impact with a large overpressure induced to it. The magnitude of the pressure was shown to depend on the size of the cluster. While the smallest clusters could vaporize and the largest remain solid, molten or partially molten [38], nanoclusters could undergo a creep deformation due to their overpressure in comparison to the molten SHI track in silica.

The existence of a threshold fluence was explained in the following manner [89]: below a certain threshold fluence, the nanoclusters grow by Ostwald ripening until a size is reached above which the nanoclusters do not evaporate upon impact, but melt and deform. This process is clearly dependent on the particle density [87].

Within this model it is not evident why the threshold fluence increases with increasing particle size. Also the origin of the correlation between the minor axis of the elongated nanoclusters and the width of the SHI track width in silicon dioxide remains unclear. The latter correlation can be better explained by considering the volume expansion of the metal nanoclusters in a molten ion track [82]. Assuming the nanoclusters can only expand within the molten track, the track width would impose the largest possible nanocluster width. Once the track width has been reached, only expansion parallel to the beam is possible. Here, it is implied that the clusters are mostly affected upon impact to the center of the cluster. It can be shown that the closer to the center of the nanocluster the ion traverses the particle, the more energy will be deposited into it [113]. Furthermore, explanations based on volume expansion are consistent with the anomaly of the transformation of Ge nanoclusters, as unlike metals, germanium densifies upon melting.

An alternate shaping mechanism was proposed in reference [100], one that depends on the ion-hammering effect [135–137]. This effect occurs on amorphisable materials and leads to an in-plane strain, which, combined with the softening of the metal clusters on irradiation,

could cause the material in the nanocluster to flow along the direction of the ion beam.

This scenario is consistent with the observation that the shape change occurs only after the silica shell was made thick enough in Au-silica core-shell nanoparticles (Ref. [111] and Fig. 12). The hypothesis gains further support by the observation that Au nanoparticles did not elongate when embedded in a crystalline AlAs matrix [99]. The observation of a threshold fluence could be explained by the effect only occurring when enough lateral stress is accumulated in the matrix. This mechanism is consistent with the observation that the threshold fluence was larger for larger nanoclusters.

Despite its success in explaining some of the experimental observations, the current theoretical work and some of the experimental observations do not support the indirect deformation model via ion hammering. In reference [102], an order of magnitude estimate using the viscoelastic model showed that lateral stress from hammering cannot be, at least alone, responsible for the shape change of any species of nanoclusters. Moreover, the MD simulations (see below) show that the shape transformation in Au nanoclusters can be explained without considering ion hammering. In reference [87], it was concluded that the deformations occur in a fluence domain not explained by ion hammering. In reference [111] it was pointed out that the electronic stopping power threshold for deformation of the nanoclusters is much higher than the hammering deformation in silica.

In addition to the ion hammering and overpressure model, it has been speculated that irradiation assisted diffusion of the ejected particles along the ion track [76] and the interfacial energies between the particle and the matrix [102] could contribute to the elongation effect, but no detailed calculations of either effect exists so far.

It should also be pointed out that a similar transformation has been seen in Ag nanoparticles embedded in glass using high intensity laser pulses [138] (elongation along the polarization direction). This effect was explained by ejection and diffusion of ionized metal atoms from the cluster, but it is not known if the deformation mechanism is related to the SHI shape transformation.

In several papers [38,83,86,93,104] the inelastic thermal spike model is applied in order to understand the experimental results. This model does not, as such, describe the transport of material, but can give insight on the timescales and importance of phase transitions on the elongation, as it can be used to predict the temperature of the nanocluster-silica system as function of particle size and time. On basis of such calculations it was reported that, assuming the elongation occurs only with the particle in the molten (or partially molten [38]) phase, the calculations are well in line with the experimental results [38,86,104].

4.2 MD simulations

To include material transport in the modeling of SHI induced effects, the MD method can be used in

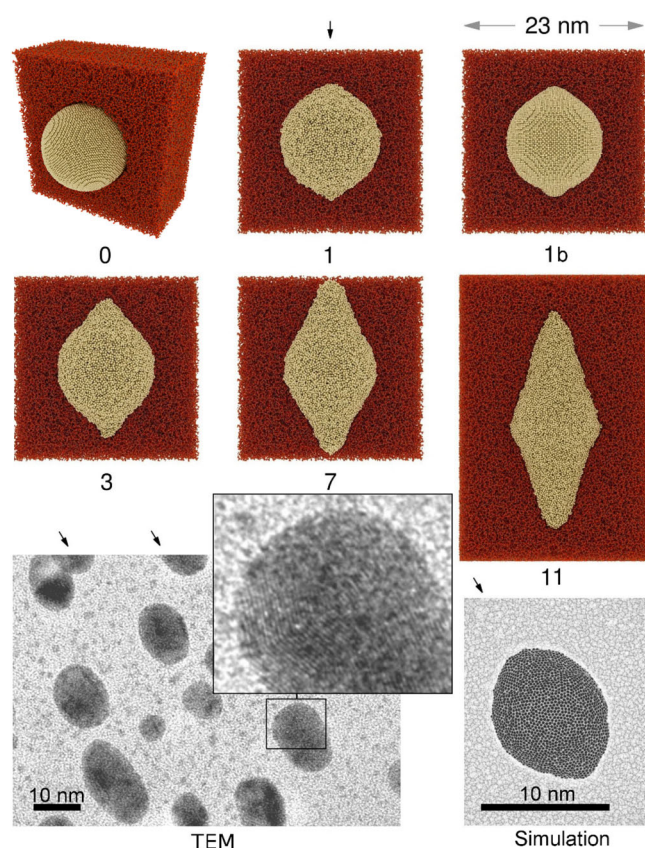


Fig. 14. Snapshots from MD simulations of nanocluster elongation. The numbers indicate the total number of impacts on the cluster and the arrows the propagation direction of the ion. Shown also the nanocluster after the recrystallization procedure (1b) and simulation results with varying ion impact positions (lower right corner). For comparison, shown also a TEM image of elongated nanoclusters (lower left). From reference [105], reprinted under the Creative Commons Attribution 3.0 License.

conjunction with the two temperature model. In the two temperature model, the thermal evolution of the atomic and electronic system is followed concurrently with an electron-phonon coupling constant used to describe the energy transfer between the two systems. Originally this was implemented numerically by solving the heat conduction equations [139–141] but more recently the atomic motion in molecular dynamics has been coupled to numerical grid solution of the electronic heat conduction [142–146] in what can be called an “MD-TTM” scheme.

The elongation of Au nanoclusters was studied using such an approach in references [105,106]. The SHI was implemented by assigning random kinetic energies to the atoms so that velocities are deduced from the initial stage of the inelastic thermal spike calculation, when the lattice temperature has reached a maximum. In spite of its relative simplicity, this approach has yielded good agreement between MD simulations and experiments in track formation calculations [147].

Using an energy deposition profile of a 164 MeV Au ion, the simulation of a direct impact of a spherical nan-

ocluster ($d = 10$ nm) led to an increase of the aspect ratio of the nanocluster to about 1.2. The elongated cluster had a “lemon” shape, similar to the experimental image in Figure 9a.

By monitoring the volume and the temperature of the nanoparticle, it was suggested that the elongation was caused by anisotropic thermal expansion of the nanocluster. This was supported by the observation that the gain in aspect ratio showed a simple correlation to the energy deposition to Au (i.e. to the temperature of the Au cluster), but a more complicated one to the deposition to silica. While at the sides of the nanocluster silica remained solid and impenetrable, the expanding material from the nanoparticle was flowing into the molten, underdense track on top and beneath the particle. After about 20 ps, the track was solidified and the elongation stopped, irrespective of the temperature of nanocluster. The saturation width was directly linked to the width of the molten, underdense region of the track in silica, as it was observed that the cluster was expanding in the perpendicular direction after impact only if the sides of the cluster were molten and underdense.

In MD simulations of additional impacts on the same cluster [105], the Au nanocluster was recrystallized in a shape-conserving way after each impact, supported by the experimental observation that the elongated nanoclusters are crystalline [123]. Using this procedure, the elongation continued on the later impacts. The behavior was explained by the differences in the pressure from the thermal expansion between the amorphous and crystalline cluster. By studying the evolution of particles of several sizes, it could also be seen that the smallest nanoparticles were not shaped as efficiently, in agreement with the experiments.

To summarize this subsection, SHI irradiation of metal nanoclusters can cause them to elongate in the ion beam direction. Decisive experiments and theory, even as to verify the basic mechanism of elongation, remains to be constructed. The majority of the articles reviewed for this article supported the idea that the effect requires melting of the nanocluster and that the molten material is then deformed by the stresses that are induced by the ions. The origin of the stress remained somewhat controversial. On one hand it was predicted that there is a large overpressure in the Au clusters after the impact, which could induce a creep deformation of the cluster into the molten track. On the other hand it was suspected that such stresses could originate from the ion-hammering effect, although calculations using the viscoelastic model or MD simulations do not support this conclusion. Recent MD simulations suggest that the driving force for the shape change is the pressure from the rapid heating of the cluster after the impact, and that that shape change can be explained in terms of molten material flow to the ion track in silica.

5 Summarizing notes

This review article has summarized the current state of understanding of interactions of beams of energetic particles with nanoclusters embedded in solids. In general

terms, the review shows that the field attracts considerable interest, from many points of view.

The largest body of work is still on the fundamental science, i.e. with the aim of determining the basic mechanisms of irradiation effects in nanoclusters, how they affect material properties, and how they differ from the bulk. In this respect, the review shows that there is in most respects good understanding, or at least quite plausible theories, for the atomic mechanisms of *primary* damage production in embedded nanoclusters. However, the longer-term damage evolution cannot be considered as well understood. For instance, it is not clear on what time scale the metal clusters irradiated by SHI's recrystallize, or what the mechanisms of damage annealing that lead to changes in luminescence are. Partly related to the previous issue, the electronic structure changes which the irradiation induces, that affect the optical and magnetic response of nanocrystals are in most cases not clear at all.

Several studies have naturally also already considered possible practical applications. In general, nanocrystals are widely used in optical applications e.g. in medical and pharmaceutical applications, and the possibility to use ion beams to tune the optical properties of embedded nanocrystals thus has clear application potential. To our knowledge no commercial applications have yet emerged from irradiation of nanocrystals, but due to the increasing use of embedded nanocrystals on one hand, and ion beams on the other, in different branches of industry, we consider it likely that such applications will eventually emerge.

Overall, this review demonstrates that the field of radiation effects in nanoclusters is interesting both from a scientific and application-oriented point of view, and that there is much exciting work that remains to be done in this field.

The authors would like to thank M. Ridgway, P. Kluth, P. Fichtner, A.V. Krasheninnikov, and K. Albe and their research groups for many years of excellent collaboration on topics related to this Review. The authors are also indebted to the Academy of Finland for the support through several projects and the Centre of Excellence programme.

References

1. C.P. Poole, F.J. Owens, *Introduction to Nanotechnology* (John Wiley & Sons, New Jersey, 2003)
2. The International Technology Roadmap for Semiconductors, available online at www.itrs.net
3. X. Huang et al., in *International Electron Devices Meeting Technical Digest, Washington, 1999*, p. 67
4. S. Tiwari, F. Rana, K. Chan, L. Shi, H. Hanafi, *Appl. Phys. Lett.* **68**, 1377 (1996)
5. S. Tiwari, F. Rana, K. Chan, L. Shi, H. Hanafi, *Appl. Phys. Lett.* **69**, 1232 (1996)
6. Report dated Jun 28, 2010 in the Web at <http://www.denali.com/wordpress/index.php/dmr/2010/06/28/new-freescale-arm-m4-and-coldfire-based>
7. The British Museum, http://www.britishmuseum.org/explore/highlights/highlight_objects/pe_mla/t/the_lycurgus_cup.aspx
8. J. Fu, G. Li, X. Mao, K. Fang, *Metall. Mater. Trans. A* **42**, 3797 (2011)
9. W.D. Callister Jr., *Materials Science and Engineering, An Introduction*, 3rd edn. (Wiley, New York, 1993)
10. D.A. Porter, K.E. Easterling, *Phase Transformation in Metals and Alloys* (Chapman & Hall, 1992)
11. A. Seeger, in *The Nature of Radiation Damage in Metals* (International Atomic Energy Agency, Vienna, 1962), Vol. 1, pp. 101–127
12. R.S. Averback, T. Diaz de la Rubia, in *Solid State Physics*, edited by H. Ehrenfest, F. Spaepen (Academic Press, New York, 1998), Vol. 51, pp. 281–402
13. S.J. Zinkle, J.T. Busby, *Mater. Today* **12**, 12 (2009)
14. L. Mansur, A. Rowcliffe, R. Nanstad, S. Zinkle, W. Corwin, R. Stoller, *J. Nucl. Mater.* **329**, 166 (2004)
15. D. Schulz-Ertner, H. Tsujii, *J. Clinical Oncology* **25**, 953 (2007)
16. M. Okamura, N. Yasuno, M. Ohtsuka, A. Tanaka, N. Shikazono, Y. Hase, *Nucl. Instrum. Methods Phys. Res. B* **206**, 574 (2003)
17. J.W. Mayer, S.S. Lau, *Electronic Materials Science For Integrated Circuits in Si and GaAs* (MacMillan, New York, 1990)
18. W. Bolse, in *International conference on beam processing of advanced materials, Cleveland, 1995*, p. 1
19. M.J. Caturla, T. Diaz de la Rubia, G.H. Gilmer, *J. Appl. Phys.* **77**, 3121 (1995)
20. K. Nordlund, R.S. Averback, *Phys. Rev. B* **59**, 20 (1999)
21. B. Weber, D.M. Stock, K. Gärtner, *Nucl. Instrum. Methods Phys. Res. B* **148**, 375 (1999)
22. K. Nordlund, J. Nord, J. Frantz, J. Keinonen, *Comput. Mater. Sci.* **18**, 283 (2000)
23. E. Wendler, B. Breger, W. Wesch, *Nucl. Instrum. Methods Phys. Res. B* **175**, 83 (2001)
24. A.V. Krasheninnikov, K. Nordlund, *J. Appl. Phys.* **107**, 071301 (2010)
25. S. Dhara, *Crit. Rev. Solid State Mater. Sci.* **32**, 1 (2007)
26. K. Nordlund, F. Djurabekova, *J. Comput. Electr.* **13**, 122 (2014)
27. K.H. Heinig, B. Schmidt, A. Markwitz, R. Grötzchel, M. Strobel, S. Oswald, *Nucl. Instrum. Methods Phys. Res. B* **148**, 969 (1999)
28. C. Bonafos et al., *J. Appl. Phys.* **95**, 5696 (2004)
29. C.W. White, J.D. Budai, S.P. Withrow, J.G. Zhu, E. Sonder, R.A. Zuhr, A. Meldrum, D.M. Hembree, D.O. Henderson, S. Praver, *Nucl. Instrum. Methods Phys. Res. B* **141**, 228 (1998)
30. P.G. Kik, A. Polman, *J. Appl. Phys.* **88**, 1992 (2000)
31. K.H. Heinig, B. Schmidt, M. Strobel, H. Bernas, in *Ion Beam Synthesis and Processing of Advanced Materials*, edited by D.B. Poker, S.C. Moss, K.H. Heinig (MRS, 2000), Vol. 647
32. F. Ren, X.H. Xiao, G.X. Cai, J.B. Wang, C.Z. Jiang, *Appl. Phys. A* **96**, 317 (2009)
33. K. Baba, T. Kaneko, R. Hatakeyama, *Appl. Phys. Express* **2**, 035006 (2009)
34. S. Dhamodaran, A.P. Pathak, D.K. Avasthi, T. Srinivasan, R. Muralidharan, D. Emfietzoglou, *Nucl. Instrum. Methods Phys. Res. B* **257**, 301 (2007)
35. L. Khriachtchev, S. Novikov, O. Kilpelä, *J. Appl. Phys.* **87**, 7805 (2000)
36. L. Khriachtchev, M. Räsänen, S. Novikov, *Appl. Phys. Lett.* **88**, 013102 (2006)

37. I.V. Antonova, A.G. Cherkov, V.A. Skuratov, M.S. Kagan, J. Jedrzejewski, I. Balberg, *Nanotechnology* **20**, 185401 (2009)
38. G. Rizza et al., *Phys. Rev. B* **86**, 035450 (2012)
39. T. Cesca, B. Kalinic, C. Maurizio, C. Scian, G. Battaglin, P. Mazzoldi, G. Mattei, *Nanoscale* **6**, 1716 (2014)
40. W. Ostwald, *Z. Elektrochem. Angew. Phys. Chem.* **22**, 289 (1897)
41. A. Flores, H. Goff, *J. Dairy, Science* **82**, 1408 (1999)
42. P. Pronk, T. Hansen, C. Ferreira, G. Witkamp, *Int. J. Refrigeration* **28**, 27 (2005)
43. G.C. Rizza, M. Strobel, K.H. Heinig, H. Bernas, *Nucl. Instrum. Methods Phys. Res. B* **178**, 78 (2001)
44. K.H. Heinig, T. Muller, B. Schmidt, M. Strobel, W. Moller, *Appl. Phys. A* **77**, 17 (2003)
45. K.A. Fichthorn, W.H. Weinberg, *J. Chem. Phys.* **95**, 1090 (1991)
46. A. La Magna, S. Coffa, L. Colombo, *Nucl. Instrum. Methods Phys. Res. B* **148**, 262 (1999)
47. A. La Magna, S. Coffa, *Comput. Mater. Sci.* **17**, 21 (2000)
48. C.C. Battaile, *Comput. Methods Appl. Mech. Eng.* **197**, 3386 (2008)
49. B. Schmidt, K.H. Heinig, A. Mucklich, *MRS Symp. Proc.* **647**, O11.20.1 (2000)
50. P. Kluth, B. Johannessen, G.J. Foran, D.J. Cookson, S.M. Kluth, M.C. Ridgway, *Phys. Rev. B* **74**, 014202 (2006)
51. G. Rizza, H. Cheverry, T. Gacoin, A. Lamas, S. Henry, *J. Appl. Phys.* **101**, 014321 (2007)
52. F. Kremer, J.M.J. Lopes, F.C. Zawislak, P.F.P. Fichtner, *Appl. Phys. Lett.* **91**, 083102 (2007)
53. F.P. Luce, F. Kremer, S. Reboh, Z.E. Fabrim, D.F. Sanchez, F.C. Zawislak, P.F.P. Fichtner, *J. Appl. Phys.* **109**, 014320 (2011)
54. D.F. Sanchez, F.P. Luce, Z.E. Fabrim, M.A. Sortica, P.F.P. Fichtner, P.L. Grande, *Surf. Sci.* **605**, 654 (2011)
55. G.A. Kachurin, M.O. Ruault, A.K. Gutakovskiy, O. Kaitasov, S.G. Yanovskaya, K.S. Zhuravlev, H. Bernas, *Nucl. Instrum. Methods Phys. Res. B* **147**, 356 (1999)
56. G.A. Kachurin, S.G. Yanovskaya, M.O. Ruault, A.K. Gutakovskii, K.S. Zhuravlev, O. Kaitasov, H. Bernas, *Semiconductors* **34**, 965 (2000)
57. S. Cheylan, N. Langford, R.G. Elliman, *Nucl. Instrum. Methods Phys. Res. B* **166-167**, 851 (2000)
58. D. Pacifici, E.C. Moreira, G. Franzo, V. Martorino, F. Priolo, F. Iacona, *Phys. Rev. B* **65**, 144109 (2002)
59. D. Pacifici, G. Franzo, F. Iacona, F. Priolo, *Physica E* **16**, 404 (2003)
60. D.I. Tetelbaum, S.A. Trushin, V.A. Burdov, A.I. Golovanov, D.G. Revin, D.M. Gaponova, *Nucl. Instrum. Methods Phys. Res. B* **174**, 123 (2001)
61. U. Serincan, M. Kulakci, R. Turan, S. Foss, T.G. Finstad, *Nucl. Instrum. Methods Phys. Res. B* **254**, 87 (2007)
62. R. Khelifi, D. Mathiot, R. Gupta, D. Muller, M. Roussel, S. Duguay, *Appl. Phys. Lett.* **102**, 013116 (2013)
63. M.C. Ridgway, G. de M. Azevedo, R.G. Elliman, C.J. Glover, D.J. Llewellyn, R. Miller, W. Wesch, G.J. Foran, J. Hansen, A. Nylandsted-Larsen, *Phys. Rev. B* **71**, 094107 (2005)
64. L.L. Araujo, R. Giulian, B. Johannessen, D.J. Llewellyn, P. Kluth, G.D.M. Azevedo, D.J. Cookson, G.J. Foran, M.C. Ridgway, *Nucl. Instrum. Methods Phys. Res. B* **266**, 3153 (2008)
65. M. Backman, F. Djurabekova, O.H. Pakarinen, K. Nordlund, L.L. Araujo, M.C. Ridgway, *Phys. Rev. B* **80**, 144109 (2009)
66. F. Djurabekova, M. Backman, K. Nordlund, *Nucl. Instrum. Methods Phys. Res. B* **266**, 2683 (2008)
67. F. Djurabekova, M. Backman, O.H. Pakarinen, K. Nordlund, L. Araujo, M. Ridgway, *Nucl. Instrum. Methods Phys. Res. B* **267**, 1235 (2009)
68. F. Djurabekova, K. Nordlund, *Phys. Rev. B* **77**, 115325 (2008), also selected to *Virtual J. Nanoscale Sci. Technol.* **17**, 13 (2008)
69. A. Kanjilal, L. Rebohle, N.K. Baddela, S. Zhou, M. Voelskow, W. Skorupa, M. Helm, *Phys. Rev. B* **79**, 161302 (2009)
70. B. Johannessen, P. Kluth, D.J. Llewellyn, G.J. Foran, D.J. Cookson, M.C. Ridgway, *Appl. Phys. Lett.* **90**, 073119 (2007)
71. R.S. Averback, K.L. Merkle, *Phys. Rev. B* **16**, 3860 (1977)
72. P. Kluth, B. Johannessen, R. Giulian, C. Schnohr, G. Foran, D. Cookson, A.P. Byrne, M. Ridgway, *Radiat. Eff. Defects Solids* **162**, 501 (2007)
73. L.G. Jacobsohn, J.D. Thompson, Y. Wang, A. Misra, R.K. Schulze, M. Nastasi, *Nucl. Instrum. Methods Phys. Res. B* **250**, 201 (2006)
74. G. Rizza, A. Dunlop, A. Dezellus, *Nucl. Instrum. Methods Phys. Res. B* **256**, 219 (2007)
75. P. Mazzoldi, G. Mattei, G. Battaglin, V. Bello, T. Cesca, S. Carturan, C.d.J. Fernandez, C. Maurizio, G. Pellegrini, C. Scian, *Radiat. Eff. Defects Solids* **168**, 418 (2013)
76. C. D'Orleans, J.P. Stoquert, C. Estournes, C. Cerruti, J.J. Grob, J.L. Guille, F. Haas, D. Muller, M. Richard-Plouet, *Phys. Rev. B* **67**, 220101 (2003)
77. H. Amekura, N. Ishikawa, N. Okubo, Y. Nakayama, K. Mitsuishi, *Nucl. Instrum. Methods Phys. Res. B* **269**, 2730 (2011)
78. H. Amekura, N. Ishikawa, N. Okubo, M.C. Ridgway, R. Giulian, K. Mitsuishi, Y. Nakayama, C. Buchal, S. Mantl, N. Kishimoto, *Phys. Rev. B* **83**, 205401 (2011)
79. H. Amekura, N. Okubo, N. Ishikawa, D. Tsuya, K. Mitsuishi, Y. Nakayama, U.B. Singh, S.A. Khan, S. Mohapatra, D.K. Avasthi, *Appl. Phys. Lett.* **103**, 203106 (2013)
80. H. Amekura, M.L. Sele, N. Ishikawa, N. Okubo, *Nanotechnology* **23**, 095704 (2012)
81. L.L. Araujo, R. Giulian, D.J. Srouster, C.S. Schnohr, D.J. Llewellyn, B. Johannessen, A.P. Byrne, M.C. Ridgway, *Phys. Rev. B* **85**, 235417 (2012)
82. D. Avasthi, Y. Mishra, F. Singh, J. Stoquert, *Nucl. Instrum. Methods Phys. Res. B* **268**, 3027 (2010)
83. K. Awazu, X. Wang, M. Fujimaki, J. Tominaga, S. Fujii, H. Aiba, Y. Ohki, T. Komatsubara, *Nucl. Instrum. Methods Phys. Res. B* **267**, 941 (2009)
84. K. Awazu, X. Wang, M. Fujimaki, J. Tominaga, H. Aiba, Y. Ohki, T. Komatsubara, *Phys. Rev. B* **78**, 054102 (2008)
85. K. Awazu, X. Wang, M. Fujimaki, J. Tominaga, H. Aiba, Y. Ohki, T. Komatsubara, *Phys. Rev. B* **78**, 054102 (2008)
86. K. Awazu, X. Wang, T. Komatsubara, J. Watanabe, Y. Matsumoto, S. Warisawa, S. Ishihara, *Nanotechnology* **20**, 325303 (2009)

87. C. D'Orléans, J. Stoquert, C. Estournès, J. Grob, D. Muller, C. Cerruti, F. Haas, Nucl. Instrum. Methods Phys. Res. B **225**, 154 (2004)
88. C. D'Orléans, C. Cerruti, C. Estournès, J. Grob, J. Guille, F. Haas, D. Muller, M. Richard-Plouet, J. Stoquert, Nucl. Instrum. Methods Phys. Res. B **209**, 316 (2003)
89. C. D'Orléans, J. Stoquert, C. Estournès, J. Grob, D. Muller, J. Guille, M. Richard-Plouet, C. Cerruti, F. Haas, Nucl. Instrum. Methods Phys. Res. B **216**, 372 (2004)
90. E.A. Dawi, A.M. Vredenberg, G. Rizza, M. Toulemonde, Nanotechnology **22**, 215607 (2011)
91. E.A. Dawi, G. Rizza, M.P. Mink, A.M. Vredenberg, F.H.P.M. Habraken, J. Appl. Phys. **105**, 074305 (2009)
92. E. Dawi, A. Klimmer, G. Rizza, P. Ziemann, Nucl. Instrum. Methods Phys. Res. B **268**, 481 (2010)
93. C. Dufour, V. Khomenkov, G. Rizza, M. Toulemonde, J. Phys. D **45**, 065302 (2012)
94. M. Gilliot, A. En Naciri, L. Johann, J. Stoquert, J. Grob, D. Muller, Phys. Rev. B **76**, 045424 (2007)
95. R. Giulian, L.L. Araujo, P. Kluth, D.J. Sprouster, C.S. Schnohr, A.P. Byrne, M.C. Ridgway, J. Phys. D **44**, 155401 (2011)
96. R. Giulian, P. Kluth, L. Araujo, D. Sprouster, A.P. Byrne, D. Cookson, M.C. Ridgway, Phys. Rev. B **78**, 125413 (2008)
97. R. Giulian, P. Kluth, D. Sprouster, L. Araujo, A.P. Byrne, M. Ridgway, Nucl. Instrum. Methods Phys. Res. B **266**, 3158 (2008)
98. R. Giulian, F. Kremer, L.L. Araujo, D.J. Sprouster, P. Kluth, P.F.P. Fichtner, A.P. Byrne, M.C. Ridgway, Phys. Rev. B **82**, 113410 (2010)
99. C. Harkati Kerboua, M. Chicoine, S. Roorda, Nucl. Instrum. Methods Phys. Res. B **269**, 2006 (2011)
100. B.S. Roorda, T.V. Dillen, A. Polman, C. Graf, A.V. Blaaderen, B.J. Kooi, Adv. Mater. **2**, 235 (2004)
101. C.H. Kerboua, J.M. Lamarre, M. Chicoine, L. Martinu, S. Roorda, Thin Solid Films **527**, 186 (2013)
102. S. Klaumünzer, Nucl. Instrum. Methods Phys. Res. B **244**, 1 (2006)
103. P. Kluth, R. Giulian, D.J. Sprouster, C.S. Schnohr, A.P. Byrne, D.J. Cookson, M.C. Ridgway, Appl. Phys. Lett. **94**, 113107 (2009)
104. H. Kumar, S. Ghosh, D.K. Avasthi, D. Kabiraj, A. Mücklich, S. Zhou, H. Schmidt, J.P. Stoquert, Nanoscale Res. Lett. **6**, 155 (2011)
105. A.A. Leino, O.H. Pakarinen, F. Djurabekova, K. Nordlund, P. Kluth, M.C. Ridgway, Mater. Res. Lett. **2**, 37 (2014)
106. A.A. Leino, O.H. Pakarinen, F. Djurabekova, K. Nordlund, Nucl. Instrum. Methods Phys. Res. B **282**, 76 (2012)
107. Y.K. Mishra, F. Singh, D.K. Avasthi, J.C. Pivin, D. Malinowska, E. Pippel, Appl. Phys. Lett. **91**, 063103 (2007)
108. S. Mohapatra, Y.K. Mishra, J. Ghatak, D.K. Avasthi, Adv. Matter. Lett. **4**, 444 (2013)
109. A. Oliver, J. Reyes-Esqueda, J. Cheang-Wong, C. Román-Velázquez, A. Crespo-Sosa, L. Rodríguez-Fernández, J. Seman, C. Noguez, Phys. Rev. B **74**, 245425 (2006)
110. V. Rodríguez-Iglesias, O. Peña-Rodríguez, H.G. Silva-Pereyra, L. Rodríguez-Fernández, G. Kellermann, J.C. Cheang-Wong, A. Crespo-Sosa, A. Oliver, J. Phys. Chem. C **114**, 746 (2010)
111. J. Penninkhof, T. van Dillen, S. Roorda, C. Graf, A. van Blaaderen, A.M. Vredenberg, A. Polman, Nucl. Instrum. Methods Phys. Res. B **242**, 523 (2006)
112. J.A. Reyes-Esqueda, V. Rodríguez-Iglesias, H.G. Silva-Pereyra, C. Torres-Torres, A.L. Santiago-Ramírez, J.C. Cheang-Wong, A. Crespo-Sosa, L. Rodríguez-Fernández, A. López-Suárez, A. Oliver, Opt. Express **17**, 12849 (2009)
113. M.C. Ridgway et al., Phys. Rev. Lett. **106**, 095505 (2011)
114. M.C. Ridgway, P. Kluth, R. Giulian, D.J. Sprouster, L.L. Araujo, C.S. Schnohr, D.J. Llewellyn, A.P. Byrne, G.J. Foran, D.J. Cookson, Nucl. Instrum. Methods Phys. Res. B **267**, 931 (2009)
115. G. Rizza, E.A. Dawi, A.M. Vredenberg, I. Monnet, Appl. Phys. Lett. **95**, 043105 (2009)
116. G. Rizza, Y. Ramjauny, T. Gacoin, S. Henry, Nucl. Instrum. Methods Phys. Res. B **257**, 15 (2007)
117. G. Rizza, F. Attouchi, P.E. Coulon, S. Perruchas, T. Gacoin, I. Monnet, L. Largeau, Nanotechnology **22**, 175305 (2011)
118. V. Rodríguez-Iglesias, O. Peña Rodríguez, H.G. Silva-Pereyra, L. Rodríguez-Fernández, J.C. Cheang-Wong, A. Crespo-Sosa, J.A. Reyes-Esqueda, A. Oliver, Opt. Lett. **35**, 703 (2010)
119. B. Schmidt, K.H. Heinig, A. Mücklich, C. Akhmadaliev, Nucl. Instrum. Methods Phys. Res. B **267**, 1345 (2009)
120. B. Schmidt, A. Mücklich, L. Röntzsch, K.H. Heinig, Nucl. Instrum. Methods Phys. Res. B **257**, 30 (2007)
121. M. Shirai, T. Horiuchi, A. Horiguchi, S. Matsumura, K. Yasuda, M. Watanabe, T. Masumoto, Mater. Trans. **47**, 52 (2006)
122. M. Shirai, K. Tsumori, M. Kutsuwada, K. Yasuda, S. Matsumura, Nucl. Instrum. Methods Phys. Res. B **267**, 1787 (2009)
123. H.G. Silva-Pereyra, J. Arenas-Alatorre, L. Rodríguez-Fernández, A. Crespo-Sosa, J.C. Cheang-Wong, J.A. Reyes-Esqueda, A. Oliver, J. Nanoparticle Res. **12**, 1787 (2009)
124. F. Singh, S. Mohapatra, J.P. Stoquert, D.K. Avasthi, J.C. Pivin, Nucl. Instrum. Methods Phys. Res. B **267**, 936 (2009)
125. F. Singh, J.C. Pivin, D. Dimova-Malinska, J.P. Stoquert, J. Phys. D **44**, 325101 (2011)
126. D.J. Sprouster, R. Giulian, L.L. Araujo, P. Kluth, B. Johannessen, D.J. Cookson, M.C. Ridgway, J. Appl. Phys. **109**, 113504 (2011)
127. D.J. Sprouster, M.C. Ridgway, Appl. Sci. **2**, 396 (2012)
128. J. Pivin, F. Singh, Y. Mishra, D. Avasthi, J. Stoquert, Surf. Coat. Technol. **203**, 2432 (2009)
129. B. Joseph, J. Ghatak, H. Lenka, P. Kuiri, G. Sahu, N. Mishra, D. Mahapatra, Nucl. Instrum. Methods Phys. Res. B **256**, 659 (2007)
130. K. Awazu, X. Wang, M. Fujimaki, J. Tominaga, H. Aiba, Y. Ohki, T. Komatsubara, Phys. Rev. B **78**, 054102 (2008)
131. H. Amekura, N. Ishikawa, N. Okubo, M.C. Ridgway, R. Giulian, K. Mitsuishi, Y. Nakayama, C. Buchal, S. Mantl, N. Kishimoto, Phys. Rev. B **83**, 205401 (2011)
132. J.C. Pivin, S. Esnouf, F. Singh, D.K. Avasthi, J. Appl. Phys. **98**, 023908 (2005)

133. D. Mohanta, G.A. Ahmed, A. Choudhury, F. Singh, D.K. Avasthi, G. Boyer, G.A. Stanciu, Eur. Phys. J. Appl. Phys. **35**, 29 (2006)
134. A. Berthelot, S. Hémon, F. Gourbilleau, C. Dufour, E. Dooryhée, E. Paumier, Nucl. Instrum. Methods Phys. Res. B **146**, 437 (1998)
135. C.A. Volkert, J. Appl. Phys. **70**, 3521 (1991)
136. E. Snoeks, A. Polman, C.A. Volkert, Appl. Phys. Lett. **65**, 2487 (1994)
137. H. Trinkaus, J. Nucl. Mater. **223**, 196 (1995)
138. A. Stalmashonak, G. Seifert, H. Graener, Opt. Lett. **32**, 3215 (2007)
139. A. Meftah, F. Brisard, J.M. Costantini, E. Dooryhee, M. Hage-Ali, M. Hervieu, J.P. Stoquert, F. Studer, M. Toulemonde, Phys. Rev. B **49**, 12457 (1994)
140. M. Toulemonde, C. Dufour, A. Meftah, E. Paunier, Nucl. Instrum. Methods Phys. Res. B **166-167**, 903 (2000)
141. M. Toulemonde, W. Assmann, C. Dufour, A. Meftah, F. Studer, C. Trautmann, Mat. Fys. Medd. Kong. Dan. Vid. Selsk. **52**, 263 (2006)
142. C. Schäfer, H.M. Urbassek, L.V. Zhigilei, Phys. Rev. B **66**, 115404 (2002)
143. D.S. Ivanov, L.V. Zhigilei, Phys. Rev. B **68**, 064114 (2003)
144. A.M. Rutherford, D.M. Duffy, J. Phys.: Condens. Matter **19**, 496201 (2007)
145. L. Koci, E.M. Bringa, D.S. Ivanov, J. Hawreliak, J. McNaney, A. Higginbotham, L.V. Zhigilei, A.B. Belonoshko, B.A. Remington, R. Ahuja, Phys. Rev. B **74**, 012101 (2006)
146. A.A. Leino, O.H. Pakarinen, K. Nordlund, F. Djurabekova, S.L. Daraszewicz, Europhys. Lett. (2014), submitted for publication
147. P. Kluth et al., Phys. Rev. Lett. **101**, 175503 (2008)